# Spectroscopic and Computational Investigations of Stable Radical Anions of Triosmium Benzoheterocycle Clusters

**Carlo Nervi,[a] Roberto Gobetto,*[a] Luciano Milone,[a] Alessandra Viale,[a] Edward Rosenberg,*[b] Dalia Rokhsana,[b] and Jan Fiedler[c]**

**Abstract:** The variable temperature $^1$H and $^{13}$C NMR and EPR spectra of the stable radical anions $[Os_3(CO)_9(\mu_3\text{-}\eta^2\text{-}L)(\mu\text{-}H)]$ (LH = phenanthridine, **1**; 5,6-benzoquinoline, **2**), and $[Os_3(CO)_{10}(\mu_3\text{-}\eta^2\text{-}L)(\mu\text{-}H)]$ (LH = quinoxaline, **3**) are reported. The radical anions $\mathbf{1}^-$, $\mathbf{2}^-$, and $\mathbf{3}^-$ can be prepared by both exhaustive electrolysis and partially by chemical reduction with cobaltocene and with sodium dispersion (only with sodium dispersion in the case of $\mathbf{3}^-$). DFT calculations on **1**–**3** reveal that the LUMO for the electron-deficient compounds **1** and **2** involves significant contributions from both the heterocyclic ligand and the two metal atoms bridged by the ligand and the μ-hydride. The character of this orbital rationalizes the previously observed regioselective reactions of these complexes with nucleophiles. In contrast, the LUMO for the electron precise **3** involves only ligand-based orbitals. Partial chemical reduction of **1** and **2** requires an excess of either cobaltocene or sodium, and their $^1$H and $^{13}$C NMR spectra reveal selective line broadening of those proton resonances that are predicted by DFT calculations to bear the greatest amount of free spin density. The variable temperature behavior of the partially chemically reduced species of **1** and **2** indicates that electron transfer between the reduced/unreduced cluster pair and between the cobaltocene/cobaltocenium pair occurs on the NMR timescale. The radical anions of **1** and **2** prepared by exhaustive electrolysis show an EPR signal at room temperature, while the NMR signals are uniformly broadened. Compound **3** appears to be partially reduced by sodium at room temperature and shows uniformly broadened $^1$H NMR resonances at room temperature that sharpen significantly at −80 °C. The temperature dependence of the spectra are discussed in terms of the effects of relative electron nuclear relaxation processes, chemical exchange, and the results of the DFT calculations.

**Keywords:** cluster compounds · electron transfer · electron-deficient compounds · osmium · radical ions

## Introduction

We have been studying the fundamental chemical properties of a series of formally electron-deficient benzoheterocycle triosmium clusters in which the electron deficiency arises from the presence of a three-center two-electron bond at the β-position with respect to the coordinated pyridinyl nitrogen (Figure 1).[1–7] The clusters are readily synthesized in moderate to good yields from $[Os_3(CO)_{10}(CH_3CN)_2]$ and the corresponding benzoheterocycle [Eq. (1)].

An interesting and useful consequence of this bonding mode is that the purported electron deficiency is apparently transmitted to the heterocycles and results in a regio- and stereoselective nucleophilic attack on the carbocyclic rings, the sites of electrophilic attack in the free ligands [Eq. (2)].[1–4] This effect, originally demonstrated for quinoline and 5,6-benzoquinoline, has now been extended to all the heterocycles in Figure 1.[8]

It is tempting to attribute the observed reactivity towards nucleophiles to contributions of the ground-state structure from resonance structures in which the cluster behaves as a classical electron withdrawing group (Scheme 1). However, in the case of the activation of $\pi\text{-}\eta^6$-arene complexes of low-valent transition metals, molecular orbital calculations suggest that there was negligible withdrawal of

[a] Prof. R. Gobetto, Dr. C. Nervi, Prof. L. Milone, Dr. A. Viale
Dipartimento di Chimica IFM, Università di Torino
via P. Giuria 7, 10125 Torino (Italy)
Fax: (+39) 011-670-7855
E-mail: roberto.gobetto@unito.it

[b] Prof. E. Rosenberg, D. Rokhsana
Department of Chemistry, University of Montana
Missoula, MT 59812 (USA)
Fax: (+1) 406-243-4227
E-mail: rosen@selway.umt.edu

[c] Ing. CSc J. Fiedler
J. Heyrovský Institute of Physical Chemistry
Academy of Sciences of the Czech Republic, Dolejškova 3
18223 Prague (Czech Republic)
Fax: (+420) 28658-2307
E-mail: jan.fiedler@jh-inst.cas.cz

Supporting information for this article is available on the WWW under http://www.chemeurj.org/ or from the author.

 DOI: 10.1002/chem.200305198  

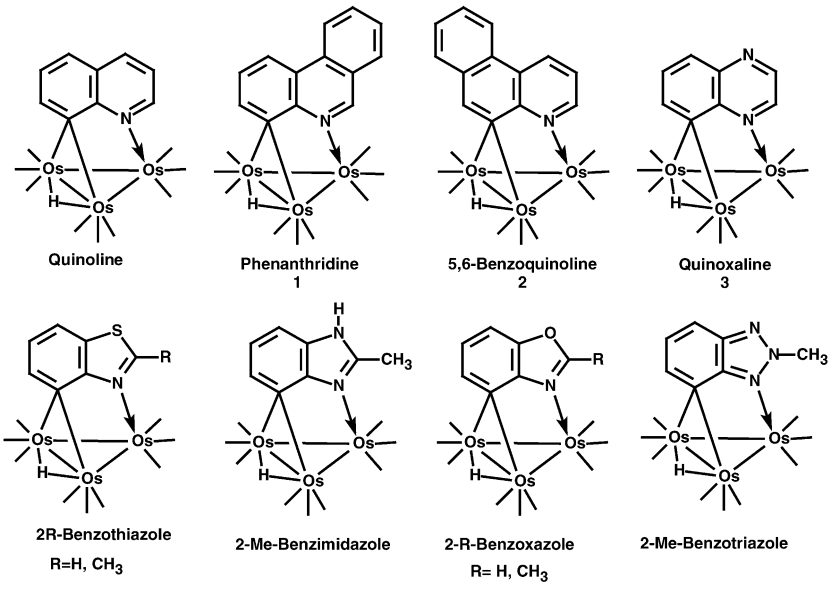


Figure 1. Structures of the family of electron-deficient benzoheterocycle triosmium clusters.

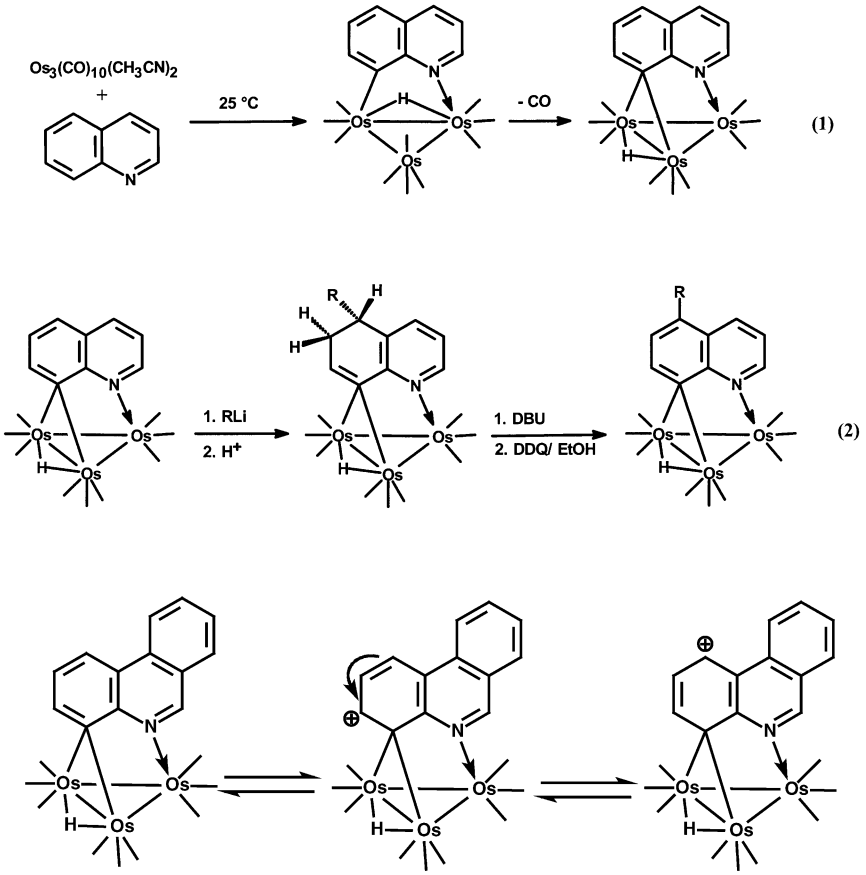


Scheme 1. Resonance structures where the triosmium cluster **1** behaves as a classical electron-withdrawing group.

electron density from the ring and that activation towards nucleophilic attack is best accounted for by orbital stabilization in the formation of the anionic intermediate following nucleophilic attack.[9] One of the objectives of the current study is to gain a better understanding of the origins of the observed nucleophilic attack [Eq. (2)] by performing molecular orbital calculations on the formally electron-deficient clusters.

A second interesting aspect of this family of clusters was revealed by the recent investigation of their electrochemical properties. All of the compounds proved to be redox active; however, in most of the complexes electrochemically reversible but chemically irreversible reductions were observed.[6] Nevertheless, in the case of the phenanthridine and 5,6-benzoquinoline complexes, **1** and **2**, respectively, very stable radical anions are obtained [Eqs. (3) and (4)].

In general, stable radical anions formed from electron-deficient clusters have the added electron localized on the metal core.[10] In the case of the clusters under consideration here, however, the ligand apparently plays a significant role in the stability of the radical anions formed from **1** and **2**. Furthermore, only one of the corresponding electron precise clusters, $[Os_3(CO)_{10}(\mu_3\text{-}\eta^2\text{-}L)(\mu\text{-}H)]$ (LH = quinoxaline, **3**), also forms a stable radical anion [Eq. (5)].[6] We felt that these observations warranted further investigation, and we report here a detailed investigation of the spectroscopic properties of the radical anions of **1**–**3**, along with molecular orbital calculations that reveal the patterns of electron distribution in these radical anions.

## Results and Discussion

**$^1$H and $^{13}$C NMR studies of the chemical reductions of compounds 1–3**: The potentials of compounds **1**–**3** in methylene chloride are −1.52, −1.44, and −1.63 V versus $FeCp_2$ (0/+1), respectively.[6] These values are in the same general range as those for polycyclic aromatic hydrocarbons and suggest that either partial or com-

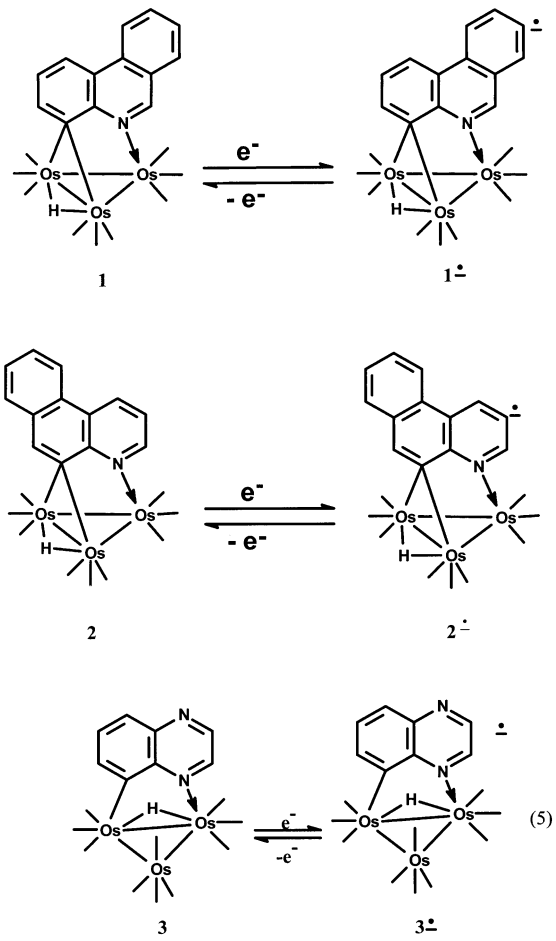


(3)

(4)

(5)

plete reduction of the radical anions of **1**–**3** could be produced by reaction with sodium or with cobaltocene, whose reduction potentials are −2.36 and −1.33 V (vs $FeCp_2$, 0/+ 1), respectively.[11,12]

The reaction of cobaltocene with **1** in a 1.4:1 molar ratio in an argon atmosphere was followed by $^1$H and $^{13}$C NMR spectroscopy. The $^1$H NMR spectrum reveals that three of the aromatic hydrogens, H2, H7, and H9, are selectively broadened with respect to the other aromatic resonances (Figure 2). The assignment of the aromatic resonances are unequivocal and are based on 2D-COSY and HMQC experiments; the calculated chemical shifts obtained from density functional theory (DFT) computations (for which the order of the chemical shifts, but not the absolute values, matched the experimental shifts). Using the reduction potentials for cobaltocenium and **1** we can calculate the homogeneous equilibrium constant at 25 °C of the reaction given in Equation (6):

$$\mathbf{1} + Cp_2Co \rightleftharpoons \mathbf{1}^- + Cp_2Co^+ \qquad (6)$$

This value is $6.1\times10^{-4}$; with a cluster concentration of $2.3\times10^{-3}$ M and the 1.4-fold excess of $CoCp_2$ used in these experiments, approximately 3 % of the phenanthridine is reduced. The approximate concentration of the radical anion is $6.7\times10^{-5}$ M. This situation parallels that in previously reported work on organic radicals whereby selective line

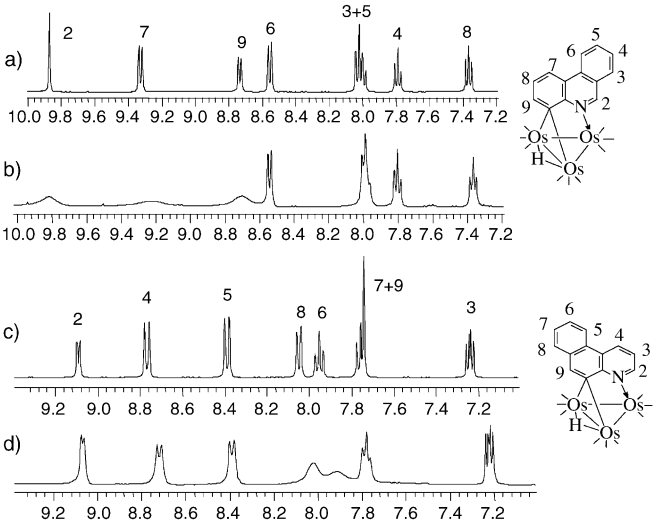


Figure 2. $^1$H NMR spectra of **1** at 400 MHz in the aromatic region a) before and b) after the addition of 1.4 equivalents of cobaltocene at ambient temperature in [$D_2$]methylene chloride; $^1$H NMR spectra of **2** at 400 MHz in the aromatic region c) before and d) after the addition of 1.5 equivalents of cobaltocene at ambient temperature in [$D_2$]methylene chloride.

broadening was also observed.[13] No resonance for the cobaltocenium ion is present, which is normally observed at 4.81 ppm. A broad peak is observed at about −40 ppm, which is likely to be the averaged cobaltocene/cobaltocenium resonance shifted to low field from that of pure cobaltocene at the same temperature. Given the low value of the equilibrium constant for this reaction, self exchange of both the phenanthridine/phenanthridine radical anion and the cobaltocene/cobaltocenium would be expected to be much faster than the cross exchange.[14] The signal from the hydride ligand is also broadened, and it is noteworthy that the degree of line broadening is different for each of the resonances. As the temperature is decreased to −80 °C all the proton resonances gradually broaden into the baseline (Figure 3). The broadening of the lines is completely reversible with the spectrum returning to its original appearance on warming to room temperature. The $^{13}$C NMR spectrum

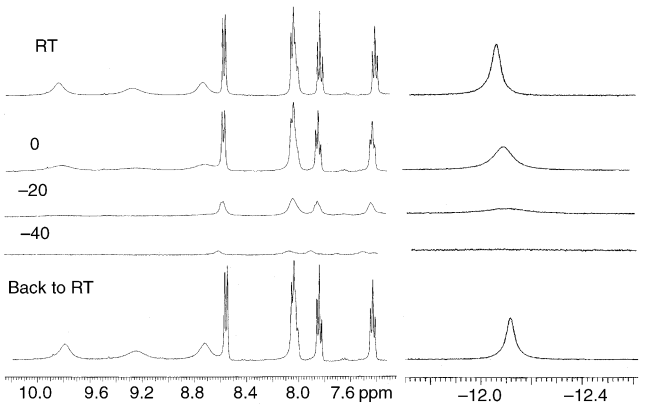


Figure 3. Variable temperature $^1$H NMR spectra of **1** at 400 MHz in the aromatic and hydride regions after addition of 1.4 equivalents of cobaltocene in [$D_2$]methylene chloride.

  

of **1**, after addition of cobaltocene (Figure 4), also shows selective line broadening of resonances attributable to C2, C7, and C9, based on assignments made from HMQC experiments and DFT calculations. However, in the case of the $^{13}C$ NMR resonances, considerable shifting of all the resonances to both high and low field is observed. When a solution of **1** in [$D_2$]methylene chloride is treated with an excess of sodium dispersion in toluene, an $^1H$ NMR spectrum almost identical to that obtained with cobaltocene is observed (Figure 5). This indicates that even with this more powerful reducing agent, reduction is not complete and the system has not reached equilibrium.

Compound **2** behaves in an analogous manner when treated with cobaltocene, but in this case the resonances assigned to H9, H6, and H8 on the basis of COSY and HMBC experiments are selectively broadened (Figure 2c and d).

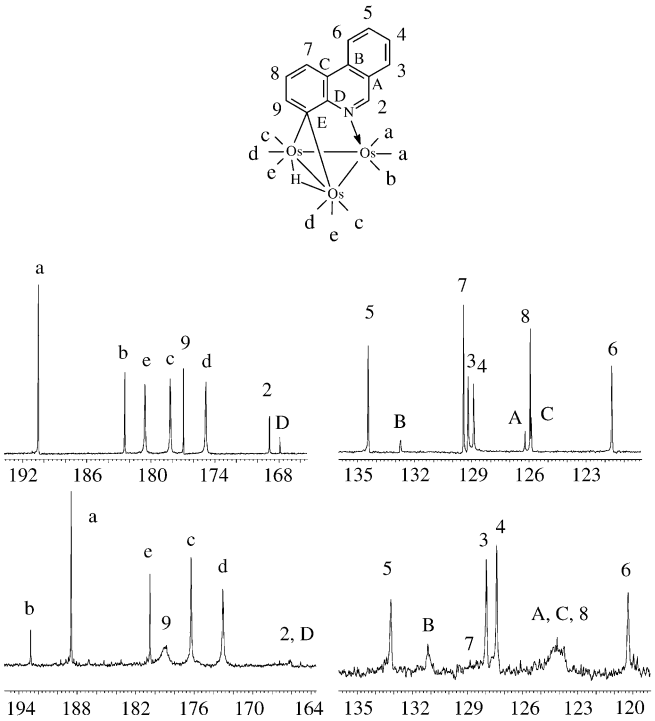


Figure 4. $^{13}C$ NMR spectra of **1** at 400 MHz in the hydrocarbon region and the carbonyl region in [$D_2$]methylene chloride at room temperature: prior to reduction with cobaltocene (upper part) and after reduction with with 1.4 equivalents of cobaltocene (lower part).

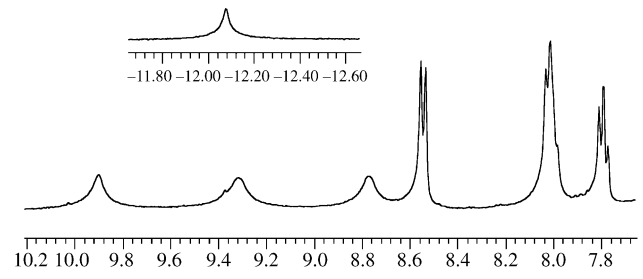


Figure 5. $^1H$ NMR spectrum of **1** at 400 MHz in the aromatic and hydride regions after reaction with sodium dispersion in toluene, in [$D_2$]methylene chloride at room temperature.

Compound **3** does not react with cobaltocene, but does undergo apparent partial chemical reduction with sodium dispersion. In sharp contrast to **1** and **2**, the $^1H$ NMR spectrum reveals uniformly broadened aromatic and hydride resonances at room temperature that sharpen as the temperature is decreased to −80 °C (Figure 6). This process is completely reversible, as all the resonances broaden again as the temperature is raised back to room temperature. That **3** reacts with sodium but not cobaltocene is not surprising, because its reduction potential is significantly more negative than that of **1** (−1.63 V).[6]

Exhaustive electrolysis of a solution of **1** in methylene chloride (5 mM) led to a completely broadened $^1H$ NMR spectrum and a well-defined ESR signal at room temperature with a *g* value of 1.99707, typical for aromatic hydrocarbon radicals.[15] This is in sharp contrast to solutions of **1** with cobaltocene, for which a broad, ill-defined ESR signal is observed at all temperatures (Figure 7).

The NMR behavior of **1**–**3** can be understood in terms of the effect of electron-transfer reactions between the neutral diamagnetic molecule and its reduced anionic paramagnetic counterpart. It has been previously reported that such electron-transfer processes can cause selective line broadening and resonance line shifts. According to the theory developed by De Boer and MacLean,[13] the electron contribution to the line width ($\Delta T_{2ex}^{-1}$) is given by the Equation (7):

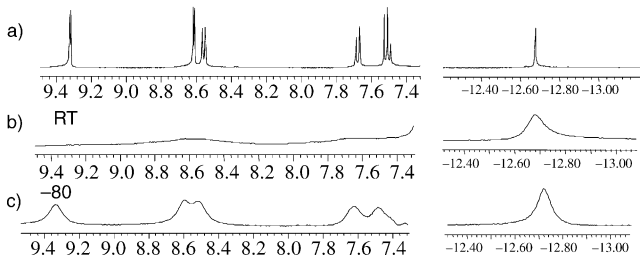


Figure 6. $^1H$ NMR spectra of **3** at 400 MHz in the aromatic and hydride regions a) before and b) after reaction with sodium dispersion in [$D_2$]methylene chloride at room temperature. c) At −80 °C after reaction with sodium dispersion.

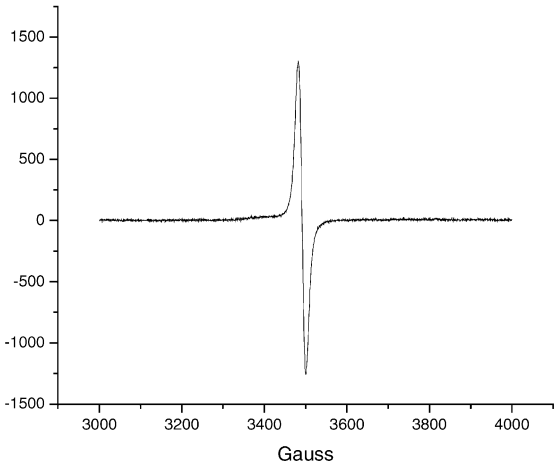


Figure 7. ESR spectrum of **1** after exhaustive electrolysis in methylene chloride at ambient temperature.

$$\Delta T_{2ex}^{-1} = \frac{f_P \tau_P a^2/4}{1 + f_D \tau_P^2 a^2/4 + 2\tau_P T_{1e}^{-1}} \quad (7)$$

in which $\tau_P$ is the lifetime of the paramagnetic molecule, $f_P$ and $f_D$ are the mole fractions of the paramagnetic and diamagnetic molecules, respectively, $a$ is the hyperfine coupling constant, and $T_{1e}$ the longitudinal relaxation of the electron. For **1** and **2**, whereby raising the temperature results in sharpening of the resonances, the rapid exchange regime applies ($f_D \tau_P^2 a^2/4 \gg 1 + 2\tau_P T_{1e}^{-1}$). Hence, the $\Delta T_{2ex}^{-1}$ is directly related to the hyperfine coupling constant and the rate of electron transfer according to Equation (8):

$$\Delta T_{2ex}^{-1} = \frac{[P]}{[D]^2} \frac{1}{4} a^2 k^{-1} \quad (8)$$

in which [P] and [D] are the concentrations of the paramagnetic and diamagnetic species, respectively, and $k$ is the rate constant for the homogeneous electron-transfer process. Significantly, the $^1$H NMR signals in **1** and **2** show different degrees of line broadening at each temperature (Figure 2). However, the ratio of the line widths for each resonance at 20 and 0 °C and at 0 and −10 °C are approximately the same for all the selectively broadened lines, including the hydride, being 2.2 and 1.5, respectively (Figure 3). Over this rather narrow temperature range the equilibrium constant and the hyperfine coupling constant would be not expected to vary very much, and one can approximate the observed line broadening to arise primarily from changes in the rate of electron transfer. We can estimate the activation energy by using the relationship given in Equation (9):

$$\ln \Delta\nu_{1/2} = \ln C + E_a/RT \quad (9)$$

in which $\Delta\nu_{1/2}$ is the change in the half height width relative to 20 °C, $C$ is an arbitrary constant, and $E_a$ is the Arrhenius activation energy. The hydride resonance of **1** provides measurable line widths at four temperatures (20, 0, −10, −20 °C, Figure 3, −10 °C not shown), and a plot of $\ln\Delta\nu_{1/2}$ versus $1/T$ gives a straight line with a correlation coefficient of 0.998, providing an estimate of $E_a = 26.5 \pm 3$ kJ mol$^{-1}$. By using a typical $A$ factor for a second-order reaction of $10^{12}$, a rate constant of $2.2 \times 10^7 \pm 0.2$ M$^{-1}$ s$^{-1}$ is calculated from the Arrhenius equation. The limited accessible temperature range and the approximations made in employing Equation (9) make this a very crude estimate of the rate of electron exchange at 20 °C, but it is not unreasonable in light of the fact that radical anions of aromatic hydrocarbons exhibit exchange rates of $\sim 10^8$ at similar temperatures.[16]

For complex **3**, partially reduced with sodium, where we observe sharpening of the resonances with decreasing temperature, the electron-transfer reaction is again the cause of the line broadening. Here, however, we are in the slow exchange regime in which $f_D \tau_P^2 a^2/4 \ll 1 + 2\tau_P T_{1e}^{-1}$ and, therefore, $\Delta T_{2ex}^{-1} = k[P]$.[13] It is worth noting that in this case the line width is independent of the hyperfine coupling constant, and uniform broadening of the resonances is expected, as observed. This is also the case for **1** after exhaustive electrolysis for which we observe a uniform sharpening of the $^1$H NMR resonances for the small amount of unreduced cluster as the temperature is decreased

**Density functional theory calculations and spectral simulations**: The density functional theory (DFT) approach has proven to be a very useful method for understanding chemical bonding in transition-metal and polymetallic complexes.[17,18] DFT methods have been previously successfully applied to calculations of triosmium clusters: Morokuma and co-workers studied the bonding in $[Os_3(CO)_9(C_6H_6)]$,[19] and Calhorda et al. studied in detail structures, frontier orbitals, and bonding of $[Os_3(CO)_{10}(\alpha\text{-diimine})]$ clusters.[20]

The most important features of the molecular-orbital description of **1** are the characteristics of the HOMO and LUMO orbitals. The HOMO is completely metal-based in character (57% contributed by the $Os_3$ core and 40% by the carbonyl ligands), while the LUMO is made up of contributions from both the metals and the ligand (13% from $Os_3$, 14% from carbonyls and the rest from the benzoheterocyclic ligand, Figure 8). Furthermore, the LUMO has a bonding interaction that involves the two metals on the same edge as the bridging hydride and C10. The distribution of the LUMO in **1** is entirely different than in the free ligand. This is particularly evident if the LUMO (0.02 e au$^{-3}$) is mapped on an electron-density isosurface (0.005 e au$^{-3}$), corresponding to the overall molecular size and shape (i.e., the van der Waals surface), for **1** and the free ligand (Figure 9). It can be seen that the positions at which the LUMO is most exposed are the 2- and 5-positions in the free ligand, while for **1** the positions that are most exposed are the 7- and 9-positions. This nicely rationalizes the

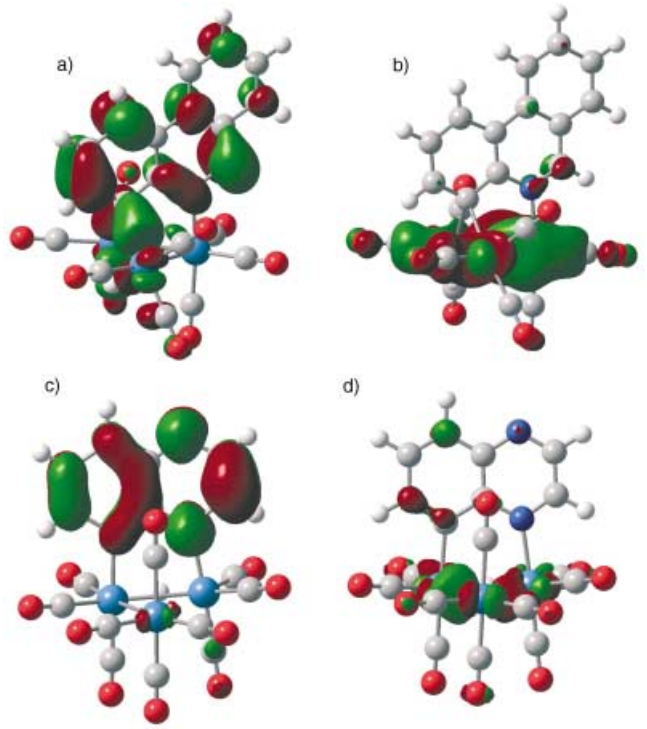


Figure 8. Drawings of molecular orbitals of the HOMO and LUMO for compounds **1** (a and b, respectively) and **3** (c and d, respectively).

  

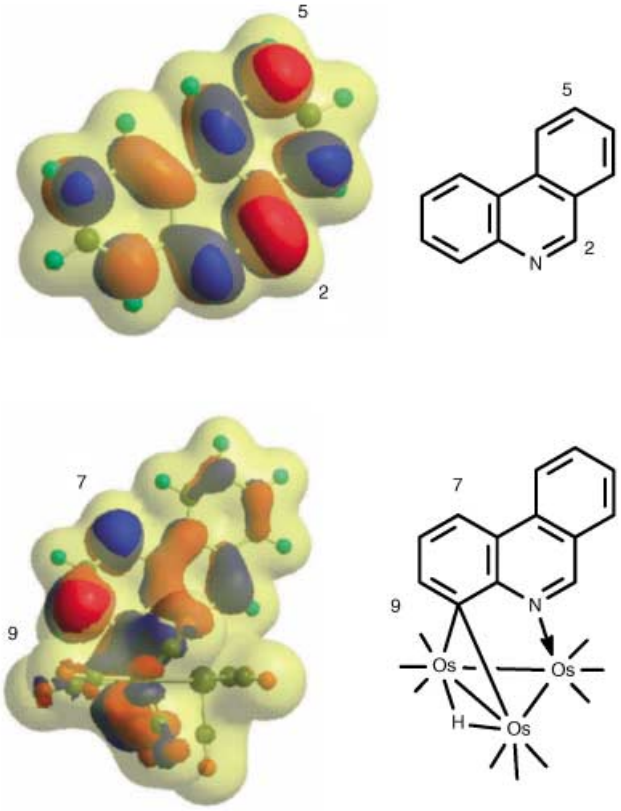


Figure 9. LUMO (0.02 e au$^{-3}$) mapped onto the electron density isosurface (0.005 e au$^{-3}$) for the free ligand phenanthridine (upper) and **1** (lower).

switching in the site of nucleophilic attack from the former positions to the latter observed experimentally on going from the free ligand to **1**, as well as in the case of quinoline.[1–3, 8] Indeed the DFT calculations give a quantum-mechanical picture that correlates with the resonance structures illustrated in Scheme 1.

DFT calculations were also preformed on **2**. The calculations predict a LUMO that is a combination of metal and ligand orbitals with a bonding interaction involving the hydride-bridged edge of the metal core and C10. DFT calculations for the free ligand predict that the LUMO will be most accessible at the 2- and 4-positions and that in **2** the most exposed LUMO sites for the free ligand are the 6- and 9-positions. These are the same sites that are observed to undergo nucleophilic attack in **2**.[4] As for **1**, the frontier-orbital model corresponds to the purported sites of electron deficiency predicted from the resonance structures in Scheme 1. In this model involvement of the hydride-bridged edge of metal core and the ligand in the LUMO replaces the idea of a formal electron deficiency as the root cause for the observed patterns of nucleophilic attack. Indeed, electron-density distributions obtained from the DFT calculations do not reveal net electron deficiencies at the observed sites of nucleophilic attack for **1** and **2**, but the shape accessibility of the LUMO is clearly indicated by the map on the electron-density isosurface, and it is this that controls the point of nucleophilic attack. This can be likened to the coefficient of the MO for the atomic orbital from which it is derived.

These results are in sharp contrast to those obtained from the DFT calculations for the formally electron precise **3**. In this case the HOMO is metal-based and the LUMO is strictly ligand-based (Figure 8). Thus the presence of the electron-deficient bonding mode in **1** and **2** has a profound effect on the character of the LUMO, which serves to connect the metal core with the ligand.

The application of the time dependent DFT (TD-DFT) methods to the study of the excited states for the interpretation of the UV/Vis spectra does not provide accurate results in some particular cases.[21] However, recent examples of the theoretical study of the ground and excited electronic states in cyclometalated phenylpyridine Ir$^{III}$ complexes show that the method can be fruitfully applied to systems containing third-row transition metals.[22] Our attempt to use the TD-DFT method to predict and assign the UV/Vis spectra to the appropriate absorption bands is summarized in Table 1. The characters of the transitions have been assigned by considering the main contributions to the transition states, and are not meant to be absolute. Not surprisingly, the transition at higher energy is metal-centered. The calculated oscillator strengths are in very good agreement with the experimental intensities of the adsorptions. The overall good agreement with the experimental data lends credence to molecular-orbital model developed by the DFT calculations.

To investigate the origin of the selective line broadening observed in **1** and **2** upon partial reduction with cobaltocene and sodium, we performed DFT calculations on the radical anions of **1** and **2**. This was done by adding one electron to the neutral molecules in their optimized geometries and performing an unrestricted B3LYP single-point energy calculation. As can be seen from the diagrams in Figure 10, the positions of maximum unpaired spin density match the positions where maximum line broadening is observed in the $^{1}$H and $^{13}$C NMR spectra of **1** and the $^{1}$H NMR spectrum of **2**. To a first approximation the unpaired spin density on a proton in a $\pi$ radical determines the magnitude of the hyperfine coupling constant.[15] If one uses the rate constant estimated for **1** and calculates the hyperfine coupling constants with Equation (8) above, the values 1.91, 2.77, and 3.63 gauss are obtained for the hydride, H2, and H7 respec-

Table 1. Experimental and calculated UV/Vis adsorption bands of **1**.

| Exptl [nm] | Calcd [nm] | Oscillator strength | Transition |
|---|---|---|---|
| 637 | 655 (1.8938 eV) | 0.0011 | *n* to σ* |
| broad adsorption | 460 (2.6934 eV) | 0.0022 | MLCT |
| around 450 | 401 (3.0894 eV) | 0.0015 | mainly MLCT |
| 380 | 380 (3.2622 eV) | 0.0132 | mainly MLCT |
| 340 | 339 (3.6541 eV) | 0.0120 | metal-to-metal (dπ-dπ) |

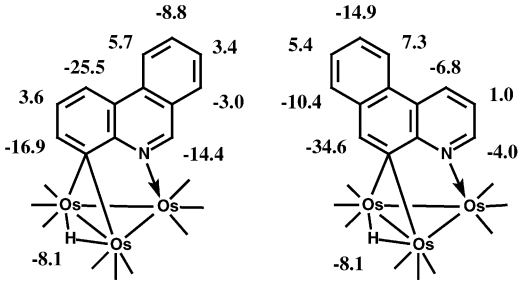


Figure 10. The scaled distribution of unpaired spin density in **1** and **2**. The numbers shown are the unpaired spin density multiplied by $10^3$. The sum of all the numbers divided by $10^3 = 1$ electron.

tively. A typical value for an aromatic radical anion is 5.34 gauss. The trend in the magnitude of the hyperfine couplings parallels the trend in the calculated spin densities, and taken together is in excellent agreement with the distribution of electron density in **1** and **2** (Figure 10).

## Conclusion

The DFT calculations reported here present a consistent picture for both the previously reported regioselective nucleophilic reactivity and the selective line broadening induced by the partial reduction of **1** and **2**. The positions in the ring at which the LUMO is most accessible are the locations where additional electron density is preferentially donated by the nucleophile and where added unpaired spin density resides. This picture coincides with that arrived at by the location of the positive formal charges resulting from the simple construction of possible resonance structures drawn with pen and paper. The electron deficient compounds **1** and **2** both show involvement of the metal core and the ligand in the LUMO, while the electron precise **3** is strictly ligand-based.

The dynamic behavior of these organometallic radical anions parallels that of the well known aromatic radical anions.[13,15] That **3** undergoes electron transfer more slowly than **1** and **2** is understandable in terms of the fact that it would be expected to be poorer acceptor of electrons, because it is electron precise. Less easy to understand is the fact that sodium, with a much more negative reduction potential, does not fully reduce either **1** or **3**. This may be related to heterogeneous nature of the solutions. In any case, we are currently investigating chemical reductions of **1**–**3** with soluble aromatic radical anions with the goal of realizing more fully reduced species. The reactivity of these species will be explored in order elucidate whether selective distribution of electron density will be manifested in regioselective reactions with spin traps and electrophiles.

## Experimental Section

**General**: Compounds were synthesized according to published literature procedures.[1–5] The NMR spectra were recorded on JEOL EX 400, Varian Unity Plus 400 MHz, and Bruker 600 MHz Avance spectrometers. The NMR solvents (Aldrich) were dried over molecular sieves (Type 4A, Mallincrodt). Chemical shifts were referenced internally relative to the residual protons in the deuterated solvents used. Temperature calibration was carried out with a methanol standard (Wilmad). DQF-COSY experiments[23] were acquired using the pulse programs available on the Varian Unity Plus 400 MHz spectrometer. The number of data points in $t_2$ was 1024 for 256 $t_1$ values, with a pulse repetition of 3 s. HMBC and HMQC experiments were run at 600 MHz. UV/Vis spectra were recorded on Perkin–Elmer Lambda 20 spectrometer. EPR were recorded on a Bruker 200 EPR spectrometer equipped with a Bruker ER031 M gauss meter and a HP 5350A microwave frequency counter.

**Electrochemistry**: Methylene chloride was distilled from calcium hydride just before use. Tetrabutylammonium hexafluorophosphate (Aldrich) was re-crystallized three times from 95% ethanol and dried in vacuum oven at 110°C overnight. Electrochemistry was performed with both a BAS CV-50W and an EG&G PAR 273 electrochemical analyzers connected to a PC, employing the software M270. Anion radicals were generated in a controlled potential (three-electrode potentiostatic) regime using a bulk electrolysis cell with mercury-pool working electrode, calomel reference electrode, and platinum counter electrode positioned in a side arm of the cell filled with the electrolyte and separated from the electrolyzed solution by sintered glass. Potential data were referred to the ferrocene (0/+1) couple,[24] which was oxidized in methylene chloride at +0.46 V verus SCE. Other experimental details were previously reported.[6]

**Calculations**: Density functional theory (DFT) calculations were performed on the triosmium clusters by using the Gaussian 98 program.[25] The NMR chemical shifts were calculated by using the gauge-including atomic orbital (GIAO) method. We used Becke's three parameter hybrid function[26] and Lee-Yang-Parr's gradient-corrected correlation function[27] ("B3LYP") throughout. The basis sets employed were LanL2DZ (Los Alamos Effective Core Potential Double-$\zeta$) for the Os atoms, with the relativistic effective core potential (ECP) which replaces the inner core electrons, and 6–311++G(d) for other atoms for all the calculations except geometry optimizations. The geometry optimizations were performed on Os with the same basis set, namely LanL2DZ, whereas for other atoms we adopted a 3–21G basis set. Geometry optimizations by using basis sets with higher quality exceeded our computational capabilities. The optimized bond lengths were within ±0.03 Å of the observed bond lengths for **1** and **2** and **3**.

## Acknowledgement

We gratefully acknowledge the support of the DOE for an EPSCoR Implementation Grant for support of this research (E.R. and D.R), the NSF EPSCOR program for visiting scholar grants (C.N. and R.G.), the COBRE Computational Core Facility at the University of Montana, and the NIH BRIN program for faculty travel award (E.R.). We also acknowledge the European Union for project COST OC D15/0001 (C.N. and J.F.) and the Italian MURST for a COFIN 2000 grant.

[1] E. Arcia, D. S. Kolwaite, E. Rosenberg, K. Hardcastle, J. Ciurash, R. Duque, R. Gobetto, L. Milone, D. Osella, M. Botta, W. Dastru, A. Viale, J. Fiedler, *Organometallics* **1998**, *17*, 415–426.
[2] M. J. Abedin, B. Bergman, R. Holmquist, R. Smith, E. Rosenberg, J. Ciurash, K. Hardcastle, J. Roe, V. Vazquez, C. Roe, S. Kabir, B. Roy, S. Alam, K. A. Azam, *Coord. Chem. Rev.* **1999**, *192*, 975–1002.
[3] B. Bergman, R. Holmquist, R. Smith, E. Rosenberg, J. Ciurash, K. Hardcastle, M. Visi, *J. Am. Chem. Soc.* **1998**, *120*, 12818–12828.
[4] R. Smith, E. Rosenberg, *Organometallics* **1999**, *18*, 3519–3527.
[5] A. Bar Din, B. Bergman, E. Rosenberg, R. Smith, W. Dastru, R. Gobetto, L. Milone, A. Viale, *Polyhedron* **1998**, *17*, 2975–2984.
[6] E. Rosenberg, M. J. Abedin, D. Rokhsana, D. Osella, L. Milone, C. Nervi, J. Fiedler, *Inorg. Chim. Acta* **2000**, *300*, 769–777.
[7] E. Rosenberg, M. J. Abedin, D. Rokhsana, A. Viale, W. Dastru', R. Gobetto, L. Milone, K. Hardcastle, *Inorg. Chim. Acta* **2002**, *334*, 343–354.

  

[8] M. J. Abedin, Ph D Thesis, University of Montana. **2002**.
[9] P. V. Schleyer, B. Kiran, D. V. Simion, T. S. Sorensen, *J. Am. Chem. Soc.* **2000**, *122*, 510–513.
[10] M. P. Brown, P. A. S. Dolby, M. M. Harding, A. J. Mathews, A. K. Smith, D. Osella, M. Arbrun, R. Gobetto, *J. Chem. Soc. Dalton Trans.* **1993**, 827–834.
[11] N. G. Connelly, W. E. Geiger, *Chem. Rev.* **1996**, *96*, 877–910.
[12] J. L. Robbins, N. Edelstein, B. Spencer, J. C. Smart, *J. Am. Chem. Soc.* **1982**, *104*, 1882–1893.
[13] E. De Boer, C. MacLean, *J. Chem. Phys.* **1966**, *44*, 1334–1342.
[14] N. Sutin, *Acc. Chem. Res.* **1968**, *1*, 225–231.
[15] J. A. Weil, J. R. Bolton, J. E. Wertz, *Electron Paramagnetic Resonance*, Wiley-Interscience, New York, **1994**.
[16] L. N. Holy, *Chem. Rev.* **1974**, *74*, 243–277.
[17] W. Koch, M. C. Holthausen, *A Chemist*'s *Guide to Density Functional Theory*, Wiley-VCH, Weinheim, **2001**.
[18] F. Jensen, *Introduction to Computational Chemistry*, Wiley, Chichester, **1999**.
[19] J. F. Rihel, N. Koga, K. Morokuma, *Organometallics* **1993**, *12*, 4788–4798.
[20] M. J. Calhorda, E. Hunstock, L. F. Veiros, F. Hartl, *Eur. J. Inorg. Chem.* **2001**, 223–231.
[21] M. Turki, C. Daniel, S. Zalis, A. Vlcek, J. van Slageren, D. J. Stufkens, *J. Am. Chem. Soc.* **2001**, *123*, 11431–11440.
[22] P. J. Hay, *J. Phys. Chem. A* **2002**, *106*, 1634–1641.
[23] M. Rance, O. W. Sørensen, G. Bodenhausen, G. Wagner, R. R. Ernst, K. Wüthrich, *Biochem. Biophys. Res. Commun.* **1983**, *117*, 479–485.
[24] W. E. Geiger, *Organometallic Radical Processes*, Elsevier, Amsterdam, **1990**, p. 144.
[25] Gaussian 98 (Revision A.9), M. J. Frisch, G. W. Trucks, H. B. Schlegel, G. E. Scuseria, M. A. Robb, J. R. Cheeseman, V. G. Zakrzewski, J. A. Montgomery, Jr., R. E. Stratmann, J. C. Burant, S. Dapprich, J. M. Millam, A. D. Daniels, K. N. Kudin, M. C. Strain, O. Farkas, J. Tomasi, V. Barone, M. Cossi, R. Cammi, B. Mennucci, C. Pomelli, C. Adamo, S. Clifford, J. Ochterski, G. A. Petersson, P. Y. Ayala, Q. Cui, K. Morokuma, D. K. Malick, A. D. Rabuck, K. Raghavachari, J. B. Foresman, J. Cioslowski, J. V. Ortiz, A. G. Baboul, B. B. Stefanov, G. Liu, A. Liashenko, P. Piskorz, I. Komaromi, R. Gomperts, R. L. Martin, D. J. Fox, T. Keith, M. A. Al-Laham, C. Y. Peng, A. Nanayakkara, C. Gonzalez, M. Challacombe, P. M. W. Gill, B. G. Johnson, W. Chen, M. W. Wong, J. L. Andres, M. Head-Gordon, E. S. Replogle, J. A. Pople, Gaussian, Inc., Pittsburgh PA, **1998**.
[26] A. D. Becke, *J. Chem. Phys.* **1993**, *98*, 5648–5652.
[27] C. Lee, W. Yang, R. G. Parr, *Phys. B* **1988**, *37*, 785.

Received: June 3, 2003 [F5198]